Atmos. Chem. Phys. Discuss., 11, 6875–6917, 2011
www.atmos-chem-phys-discuss.net/11/6875/2011/
doi:10.5194/acpd-11-6875-2011

Atmospheric Chemistry and Physics Discussions

High-resolution simulations of atmospheric CO_2 over complex terrain – representing the Ochsenkopf mountain tall tower

D. Pillai[1], C. Gerbig[1], R. Ahmadov[2,3], C. Rödenbeck[1], R. Kretschmer[1], T. Koch[1], R. Thompson[1,4], B. Neininger[5], and J. V. Lavrič[1]

[1]Max Planck Institute of Biogeochemistry, Jena, Germany
[2]NOAA Earth System Research Laboratory, Boulder, Colorado, USA
[3]Cooperative Institute for Research in Environmental Sciences, University of Colorado, Boulder, USA
[4]Laboratoire des Sciences du Climat et l'Environnement (LSCE), UMR8212, Gif-sur-Yvette, France
[5]MetAir AG, Flugplatz, 8915 Hausen am Albis, Switzerland

Received: 20 December 2010 – Accepted: 18 February 2011 – Published: 1 March 2011

Correspondence to: D. Pillai (kdhanya@bgc-jena.mpg.de)

Published by Copernicus Publications on behalf of the European Geosciences Union.

Abstract

Accurate simulation of the spatial and temporal variability of tracer mixing ratios over complex terrain is challenging, but essential in order to utilize measurements made in complex orography (e.g. mountain and coastal sites) in an atmospheric inverse framework to better estimate regional fluxes of these trace gases. This study investigates the ability of high-resolution modeling tools to simulate meteorological and CO_2 fields around Ochsenkopf tall tower, situated in Fichtelgebirge mountain range – Germany (1022 m a.s.l.; 50°1′48″ N, 11°48′30″ E). We used tower measurements made at different heights for different seasons together with the measurements from an aircraft campaign. Two tracer transport models – WRF (Eulerian based) and STILT (Lagrangian based), both with a 2 km horizontal resolution – are used together with the satellite-based biospheric model VPRM to simulate the distribution of atmospheric CO_2 concentration over Ochsenkopf. The results suggest that the high-resolution models can capture diurnal, seasonal and synoptic variability of observed mixing ratios much better than coarse global models. The effects of mesoscale transports such as mountain-valley circulations and mountain-wave activities on atmospheric CO_2 distributions are reproduced remarkably well in the high-resolution models. With this study, we emphasize the potential of using high-resolution models in the context of inverse modeling frameworks to utilize measurements provided from mountain or complex terrain sites.

1 Introduction

It is well known that atmospheric CO_2 is rising due to fossil fuel combustion and deforestation. Being the most important anthropogenic greenhouse gas, accumulation of CO_2 in the atmosphere is reported to be the major cause of global warming (Le Treut et al., 2007). Out of the total emitted CO_2, about 55% is taken up by natural reservoirs (the land biosphere and ocean), while the rest, the so-called "airborne fraction", stays in the atmosphere. However, this fraction exhibits large interannual variability due to the varying source and sinks of CO_2, mainly over land. Quantifying these sources and

ACPD
11, 6875–6917, 2011

sinks is highly demanded in predicting future increases in atmospheric CO_2 to a high degree of certainty. This requires profound understanding of natural process involved in sequestrating carbon and their variability. Furthermore, it is essential to understand the feedback mechanisms between the carbon cycle and the global climate system to enable, in the near future, the implementation of emission reduction and sequestration strategies towards mitigating adverse effects of climate change.

Two approaches are currently used to infer the source-sink distribution of CO_2 globally, namely the bottom-up and top-down methods. In the bottom-up approach, the local scale process information, such as that obtained from eddy covariance towers, is scaled-up using diagnostic or process-oriented models in combination with remote sensing measurements to derive net CO_2 exchanges between the land surface and the atmosphere on regional or global scales. However, the accuracy of this approach relies on the representativeness of the local flux measurement site, hence one can expect significant uncertainties due to the extrapolation of non-representative eddy flux tower measurements. On the other hand, in the top-down approach, the variability in atmospheric CO_2 concentrations are observed to better understand the causes of variability in the source/sink distribution by inverting the atmospheric transport matrix (inverse modeling). The scarcity of concentration data and uncertainties in simulating atmospheric transport can introduce large uncertainties in this approach.

A number of studies used inverse modelling tools at global and regional scales (Enting, 1993; Tans et al., 1990; Jacobson et al., 2007; Rödenbeck et al., 2003; Gurney et al., 2002; Gourdji et al., 2008; Lauvaux et al., 2008) together with global networks of observations, which also recently include tall tower observatories, to calculate the source-sink distribution of CO_2. Tall tower observatories sample the lower atmosphere over continents up to altitudes of 200 m or more, and the resulting CO_2 concentration profiles provide information on regional fluxes. In order to better resolve the responses of various vegetation types and the impact of human interventions (land use change and land management) on land-atmosphere fluxes, inversions need to focus on smaller scales and to utilize continental (non-background) measurements of CO_2. This

ACPD
11, 6875–6917, 2011

becomes problematic since the aforementioned in-situ measurements are often influenced by strongly spatially and temporally varying surface fluxes (fossil fuel emissions and biosphere-atmosphere exchange) in the near field and by mesoscale transport phenomena, thus reducing their scale of representativeness to about 100 km (Gerbig et al., 2009).

Mountain sites, on the other hand, provide measurements with larger scale representativeness compared to measurements made from towers over flat terrain. Moreover, the longest greenhouse gas records are often from mountain sites (e.g., Schauinsland in Germany and Monte Cimone in Italy) (Levin et al., 1995; Reiter et al., 1986), making them a valuable ingredient for assessing longer term variations in carbon budgets. However, the mesoscale atmospheric transports at these sites such as mountain-valley circulations and terrain induced up-down slope circulations are found to have a strong influence on the atmospheric distribution of trace gas mixing ratios (Gangoiti et al., 2001; Pérez-Landa et al., 2007; van der Molen and Dolman, 2007). These significant variations of atmospheric concentrations appear at relatively small scales that are not resolved by current global transport models used in inversions, complicating the interpretation of these measurements. The unresolved variations can introduce significant biases in flux estimates and renders the flux estimation strongly site-selection dependent, sometimes causing the net annual sink strength of a whole continent to change by nearly a factor two (Peters, 2010). A model inter-comparison study over Europe, using various transport models with different horizontal and vertical resolutions, suggested that the fine-scale features are better resolved at increased horizontal resolution (Geels et al., 2007). Moreover, the study of (Geels et al., 2007) discusses the limitations of using atmospheric concentration data from mountain stations in inversions due to the model's (both global and regional scale models) inability to represent complex terrain and to capture mesoscale flow patterns in mountain sites. Therefore, inversion studies usually tend to exclude the data from mountain or complex terrain sites, impose less statistical weighting (larger uncertainty), or implement temporal data filtering to the measurements (e.g. selection of nighttimes only data at mountain sites).

ACPD
11, 6875–6917, 2011

The effect of transport errors on tracer concentrations are investigated in many studies (Lin and Gerbig, 2005; Gerbig et al., 2008; Denning et al., 2008) and the uncertainties for modeled mixing ratios during growing seasons due to the difference in advection and vertical mixing, can be as large as 5.9 ppm (Lin and Gerbig, 2005) and 3.5 ppm (Gerbig et al., 2008), respectively. Thus, it is pertinent to minimize these large and dominant uncertainties in inverse modeling systems. One approach would be to increase the spatial resolution of the models in order to capture the "fine-structures" as well as to use improved boundary layer schemes to better represent the vertical mixing. Furthermore, fluxes in the near-field of the observatories are highly variable, calling for a-priori fluxes to be specified at high spatial resolution. Detailed validations of such high-resolution forward models using networks of atmospheric measurements are needed to assess how well the transport and variability of atmospheric tracers are represented. A number of studies using high-resolution models for resolving mesoscale transport in the atmosphere showed substantial improvements in simulating atmospheric CO_2 concentrations under various mesoscale flow conditions (Ahmadov et al., 2009; Sarrat et al., 2007; van der Molen and Dolman, 2007; Tolk et al., 2008).

This paper uses high-resolution modeling tools together with airborne campaign measurements to address the representativeness of greenhouse gas measurements at one particular mountain site, the Ochsenkopf station. A 163 m tall tower at Ochsenkopf, continuously monitoring CO_2 and other trace gases, is located in the second highest peak of Fichtelgebirge mountain range (1022 m a.s.l.; 50°1′48″ N, 11°48′30″ E) in Germany (Fig. 1). The site has complex terrain (Fig. 1b), where slopes influence atmospheric transport and consequently the observed mixing ratios (Thompson et al., 2009). Due to the difficulties in interpreting these measurements, the Ochsenkopf data were excluded in the global inversions of (Rödenbeck, 2005; Peters, 2010). A modeling framework consisting of a high-resolution Eulerian transport model, Weather Research Forecast (WRF) (http://www.wrf-model.org/) coupled to a diagnostic vegetation model, Vegetation Photosynthesis and Respiration Model (VPRM) (Mahadevan et al., 2008) is used to assess whether measurements can be represented sufficiently well

ACPD
11, 6875–6917, 2011

when increasing the models' spatial resolution. The coupled model, WRF-VPRM (Ahmadov et al., 2007) simulates CO_2 concentrations at high spatial resolution using high-resolution CO_2 fluxes from net ecosystem exchange (NEE) and from fossil fuel emissions. In addition, a Lagrangian particle dispersion model, Stochastic Time-Inverted Lagrangian Transport Model (STILT) (Lin et al., 2003), driven with high-resolution assimilated meteorological fields, is used to simulate the upstream influence on the observation point (i.e. the footprints), which are then multiplied by VPRM fluxes (NEE) as well as fluxes from fossil fuel emissions in order to simulate CO_2 concentrations at the observation location. When the transport is adequately represented, the footprints calculated in the modeling system can be used to retrieve the source-sink distribution from CO_2 measurements over complex terrain at much higher spatial and temporal resolution than achievable with current global models.

The main goals of this study are: (1) to test the ability of high-resolution modeling tools to represent the spatial and temporal variability of CO_2 over complex terrain, compared to coarser models, (2) to infer the effect of mesoscale flows, such as mountain-valley circulations and mountain wave activities, on the observed atmospheric CO_2 fields and to assess how well these are reproduced in the high-resolution models, (3) to evaluate the models' reproducibility in capturing synoptic, seasonal and diurnal variability of observed CO_2 concentrations and (4) to assess the possibility of using these measurements in future inversion studies. The paper is structured as follows: Sect. 2 describes briefly the data and the model set-up. In Sect. 3, the simulations from our high-resolution modeling framework are presented together with the observations as well as global model simulations. These results are discussed and conclusions are given in Sects. 4 and 5.

ACPD
11, 6875–6917, 2011

2 Data and modeling system

2.1 Tower and airborne measurements

The Ochsenkopf tall tower (from now on referred to as OXK) was instrumented as part of the European project – CHIOTTO (Continuous High-precision Tall Tower Observations of greenhouse gases) to establish a tall tower observation network for the continuous monitoring of the most important greenhouse gases over the European continent. The tower has been operated by the Max Planck Institute for Biogeochemistry, Jena, for continuous measurements of CO_2, CH_4, N_2O, CO, SF_6, O_2/N_2, and isotopes, in addition to meteorological parameters, and after re-equipping with instruments data are available since the beginning of 2006 (Thompson et al., 2009). For this study, we used high precision (±0.02 ppm) CO_2 measurements made at three heights (23 m, 90 m and 163 m) on OXK for different seasons. CO_2 is sampled at 2-min intervals from all three heights in a 3-h cycle with 1 h for each height. The meteorological observations from the tower: temperature and relative humidity at 90 m and 163 m, pressure at 90 m, and wind speed and direction at 163 m, are also analyzed.

Measurements from wind profilers can be used to infer the state of air flow and dynamics within the tropospheric column. These can be used to evaluate the model in predicting vertical gradients of meteorological variables, which are associated with the transport of tracer constituents in the atmosphere. For this purpose, wind profiler measurements at Bayreuth, Germany (49.98° N, 11.68° E, 514 m a.s.l, http://www.metoffice.gov.uk/science/specialist/cwinde/profiler/bayreuth.html) are used. These comparisons shall give insight into the mesoscale flow patterns around OXK and help assess how well these are represented in the model.

Apart from tower-based data, we used the measurements from an airborne campaign with the METAIR-DIMO aircraft (http://www.metair.ch/) over Ochsenkopf. The high precision aircraft measurements, sampling air horizontally and vertically, are designed to understand the regional patterns of CO_2, the influence of surface fluxes in the near-field, as well as atmospheric mesoscale transport and vertical mixing. In particular

ACPD
11, 6875–6917, 2011

at Ochsenkopf, it is necessary to assess the influence of terrain-induced circulations on the mixing of atmospheric trace gases, which would create errors in inverse estimates of fluxes. The campaign was carried out during October 2008, covering an area around OXK (see Fig. 1) where the air was sampled for species such as CO_2, CO and meteorological parameters, such as wind velocity, pressure, relative humidity and potential temperature, were measured. The boundary layer, up to several kilometers upwind of Ochsenkopf, was probed with multiple profiles during these flights. The fast and accurate measurement of CO_2 was achieved with an open path IRGA LI-7500 (greenhouse-gas analyzer), fitted to a LICO2 (modified closed path IRGA LI-6262) and then to flask samples, with a resolution of 20 Hz, which was down-sampled to 10 Hz to give an accuracy of better than 0.5 ppm. For more details about measuring systems, see http://www.metair.ch/.

2.2 Modeling system

We used two high-resolution transport models WRF (Eulerian) and STILT (Lagrangian), coupled to a biosphere model, VPRM, to simulate distribution of atmospheric CO_2. Both of these coupled models, WRF-VPRM and STILT-VPRM were provided with same high-resolution surface fluxes as well as initial tracer concentrations at the boundaries.

VPRM computes biospheric fluxes (NEE) at high spatial resolution by using MODIS satellite indices (http://modis.gsfc.nasa.gov/), i.e. Enhanced Vegetation Index (EVI) and Land Surface Water Index (LSWI), and simulated WRF meteorological fields, i.e. temperature at 2 m and short wave radiation fluxes. VPRM uses eight vegetation classes with different parameters for each class to calculate CO_2 fluxes. These parameters were optimized against eddy flux measurements for different biomes in Europe collected during the CarboEurope IP experiment (http://www.carboeurope.org/). Further details on VPRM can be found in (Mahadevan et al., 2008).

High-resolution fossil fuel emission data, at a spatial resolution of 10 km, are prescribed from IER (Institut für Energiewirtschaft und Rationelle Energieanwendung), University of Stuttgart, Germany (http://carboeurope.ier.uni-stuttgart.de/) to account

ACPD
11, 6875–6917, 2011

for anthropogenic fluxes. Initial and lateral CO_2 tracer boundary conditions are calculated by a global atmospheric Tracer transport model, TM3 (Heimann and Koerner, 2003), with a spatial resolution of $4^\circ \times 5^\circ$, 19 vertical levels and a temporal resolution of 3 h. We use analyzed CO_2 fields (available at http://www.bgc-jena.mpg.de/~christian.roedenbeck/download-CO2-3D/) that are consistent with atmospheric observations at many observing stations around the globe, generated by the forward transport of previously optimized fluxes (i.e. by an inversion).

In the coupled model, WRF-VPRM, the domain is set up for a small region ($\sim 500 \times 500\,km^2$, hereafter referred as "WRF domain") centered over the OXK, and is nested with a horizontal resolution of 6 km (parent) and 2 km (nested) as well as with 41 vertical levels (thickness of the lowest layer is about 18 m) (Fig. 1a). Each day of simulation starts at 18 UTC of the previous day, and continues with hourly output for 30 h of which the first 6 h are used for meteorological spin-up. CO_2 fields for each subsequent 30-hour run are initialized after the meteorological spin up with the previous day's final CO_2 fields. The coupled model STILT-VPRM (Matross et al., 2006) is set up with a domain covering most of Europe, and virtual particles were transported backward in time for a maximum of 15 days. Trajectories were driven with WRF meteorology until particles left the WRF domain, and with ECMWF (http://www.ecmwf.int/) meteorology (horizontal resolution of approximately 25 km) for the rest of the domain. The sub-grid scale turbulence in STILT-VPRM is modeled as stochastic Markov chain. In STILT-VPRM, receptors are either located at different measurement levels on the tower or at different altitudes covering the flight track of the aircraft. The vertical mixing height (zi) is slightly different in WRF and STILT, although the same meteorological (for the STILT nested domains) and surface flux fields were used (see Sect. 3.1.1 in Pillai et al., 2011). For more detailed information on these coupled models (WRF-VPRM and STILT-VPRM), the reader is referred to (Ahmadov et al., 2007; Nehrkorn, 2010; Pillai et al., 2011). Note that STILT-VPRM uses a different model domain (Europe) than WRF-VPRM, using additional meteorological information from ECMWF outside the WRF domain as mentioned above.

ACPD
11, 6875–6917, 2011

A continuous record of meteorological fields and CO_2 concentrations from a tower allows the evaluation of models for different seasons as well as for different measurement levels. Model simulations were carried out for May (spring), August (summer), October (autumn) in 2006, and March (winter) in 2008. In addition to this, simulations were carried out for October 2008 in order to evaluate the models against the DIMO aircraft measurements to assess the model's ability to reproduce CO_2 distributions over the Ochsenkopf mountain region.

3 Results

Here we present high-resolution simulations of meteorology (by WRF) and CO_2 (by WRF-VPRM and STILT-VPRM) at 2 km resolution around OXK. The models are evaluated using wind profiler, tower and airborne measurements of meteorological parameters and CO_2 concentrations. These model evaluations assess the ability of the high-resolution model framework to simulate atmospheric transport and to capture the spatial and temporal variability of atmospheric CO_2.

3.1 Model evaluation: meteorology

3.1.1 Wind profiler

Vertical profiles of meteorological fields are validated for 2 to 30 August 2006 with the measurements provided by the Bayreuth wind profiler, located about 10 km south-west of OXK. For demonstration, a comparison of measured and modeled wind and temperature profiles on 3 August 2006 at 15:00 UTC is shown in Fig. 2a,b. The observed prevailing wind direction was northerly for the atmospheric column below 2 km which was also reproduced by the model simulation. For a thin vertical layer, between 2.3 and 3.2 km, the prevailing wind direction changed to south-east; however the model simulated a north-westerly wind. Above 3.2 km, both observations and simulations

ACPD
11, 6875–6917, 2011

indicated a south-westerly wind. The magnitude of the wind was slightly overestimated in the model, particularly in the boundary layer (bias: $\sim +2\,\mathrm{m\,s^{-1}}$).

An observation-model comparison of the vertical profile of virtual potential temperature (θv) showed that the model simulates θv reasonably well, but with a warm bias. A relatively sharp decrease in θv for the thin vertical layer between 2.3 and 3.2 km could not be captured in the model. A possible reason for the decrease in θv could be the intrusion of air from south-east direction on this layer (see Fig. 2a for wind direction) that existed for a short period of time.

To analyze the overall agreement, the monthly averages of profiles for wind-speed and θv, both measured and simulated, are produced at 15:00 UTC and the data-model mismatches are shown in Fig. 2c,d. The result shows that the model slightly overestimated wind-speed in the boundary layer and in contrast showed an underestimation for the free troposphere. In general, the model slightly underestimated θv profiles. Overall, the model could capture much of the variability in the vertical profiles of wind-speed and θv.

3.1.2 Tower

Evaluations of the modeled meteorology are carried out at different measurement levels on the tower for different seasons. An example of those validations is demonstrated here. Figure 3 shows time series' of observed and WRF-simulated parameters (temperature, relative humidity and wind components) for August 2006. The plot shows the prevailing weather situation and also the model capability to predict these parameters, which can drive atmospheric CO_2 variability over OXK.

Simulated atmospheric temperatures at two different levels (90 m and 163 m) on the tower agree well with observations (squared correlation coefficient, $R^2 = 0.86$) (Fig. 3a,b) and captured reasonably well the diurnal variability of temperature. Note that the model layers relative to the model terrain are used for all comparisons unless otherwise mentioned. A warm bias is observed at OXK during this period while there is a cold bias at Bayreuth (wind profiler). This good temperature agreement suggests

ACPD
11, 6875–6917, 2011

that uncertainties in the (simulated) temperature dependent VPRM respiration fluxes caused by temperature biases are expected to be small on synoptic time scales.

The transport of moisture (comparable to CO_2 transport) in the model was validated by comparing the measured and simulated relative humidity at two levels. The model agrees well with the observations ($R^2 = 0.60$–0.74) with a slight negative bias of 0.2 to 4.7 between levels (Fig. 3c,d).

The wind speed and direction was also predicted reasonably well. A comparison of horizontal components of observed and modeled wind components u (east-west) and v (north-south) at 163 m (Fig. 3e,f) demonstrates fairly good agreement between observations and simulations ($R^2 = 0.70$ and 0.61, respectively).

Table 1 gives the overall model performance (model bias, standard deviation of model-data mismatch and squared correlation coefficient of the model-data agreement) from comparing the hourly time series of observed and simulated meteorological fields at the available measurement levels for different seasons. The summary statistics indicate that WRF could follow reasonably well the seasonal changes in the atmospheric transport and dynamics.

3.1.3 DIMO campaign

Vertical distributions of meteorological fields were validated against the DIMO profiles around the Ochsenkopf mountain region for all campaign days. The box-whisker plot (Fig. 4a,b) of the data-model mismatch (from all aircraft profiles) provides an overview of the model performance on simulating specific humidity and wind speed. In general, WRF meteorological simulations agree well with the DIMO observations as indicated by the lower median ($+0.25\,g\,kg^{-1}$ for water-vapor mixing ratio and $-0.06\,m\,s^{-1}$ for wind speed while using all available observations and simulations) and 95% quartile ($1.5\,g\,kg^{-1}$ for specific humidity and $3.2\,m\,s^{-1}$ for wind speed). Noteworthy is that the data-model mismatch for water vapor mixing ratio increases with increasing height.

As an example, we demonstrate the model-data comparison for 19 October 2008 from 10:00 to 14:00 UTC. During this period, the air was sampled intensively near

ACPD
11, 6875–6917, 2011

the top of OXK and the surrounding mountain ridges and valleys (Fig. 5c). Figure 5 shows the vertical cross-section of the observed and modeled meteorological fields (wind speed and specific humidity) as a function of distance flown by the aircraft (Cumulative Distance, hereafter referred to simply as distance). WRF reproduced specific humidity fairly well at the surface layers; however, it showed a slight underestimation in the upper vertical levels (Fig. 5a,b). A relatively calm wind (2–5 m s^{-1}) was observed over Ochsenkopf mountain ranges during this period except in the early hours of the campaign. This was predicted remarkably well in WRF with negligible bias (Fig. 5c,d).

3.2 Model evaluation: CO_2 concentrations

Similar to Sect. 3.1, here we use observations of CO_2 fields at OXK and during the DIMO aircraft campaign for the evaluation of the models (WRF-VPRM and STILT-VPRM).

3.2.1 Tower

The observed atmospheric CO_2 concentrations at different measurement levels are compared with simulations generated by WRF-VPRM and STILT-VPRM for different seasons. For illustration, we show the time series comparison of CO_2 concentrations at 90 m level on the tower for the period from 2 to 30 of August 2006 (Fig. 6). The period is chosen due to its enhanced biospheric activity and the existence of strong diurnal patterns in transport and fluxes which can complicate the measurement interpretation. For comparison, the CO_2 analyzed fields from TM3 with 3-h time steps are also included. The observed atmospheric CO_2 shows large diurnal and synoptic variability and notably, these large variations in atmospheric CO_2 were not captured in the TM3 global model. Note that the generation of analyzed CO_2 fields (by atmospheric inversion) did not include OXK CO_2 data, so in this sense they can be used for independent validation. The comparison becomes more favorable when high-resolution transport and fluxes are used. Most of the observed variability in CO_2 concentrations

ACPD
11, 6875–6917, 2011

on the tower is reproduced well in both high-resolution models when compared to TM3 (Fig. 6). This points to the fact that most of the variations in CO_2 are due to surface flux variations and mesoscale transport processes on scales not resolved by TM3, which has a grid-cell size of several hundred kilometers. Also note that TM3 uses coarse resolution terrain elevation data.

In addition to August (summer) 2006, CO_2 concentrations are also validated for other seasons and the summary statistics (similar to Table 1) of the model-data comparison are given in Table 2. Observations from other levels (23 m and 163 m) on the tower are also used to assess the models' performance in reproducing the vertical structure of CO_2 in the atmospheric column. The summary statistics clearly indicate that high-resolution models are able to predict remarkably well the temporal patterns of CO_2, measured at three different vertical levels on the tower, for different seasons. Section 3.2.4 discusses further the seasonal variability of CO_2 concentrations.

3.2.2 DIMO campaign

The profiles of atmospheric CO_2 concentrations obtained from the aircraft campaign were used to examine how well the models can reproduce the vertical distribution of tracer concentrations over the Ochsenkopf mountain region. Figure 4c shows the statistical analysis of data-model mismatches using CO_2 profiles for all days in the campaign. The median of all residuals is 0.5 (1.1) ppm for STILT-VPRM (WRF-VPRM). The data-model mismatch of CO_2 for both models increases with decreasing heights, the opposite of what was found for water vapor. The reason is twofold: (1) the large variability of CO_2 at the surface compared to higher levels (Pillai et al., 2010) and (2) improper representation of boundary layer vertical mixing in the models.

The same period that was chosen for DIMO meteorological validations is used also here as an example to demonstrate the vertical distribution of CO_2. Figure 7 shows the vertical cross section of the observed and simulated CO_2 concentration as a function of distance for 19 October 2006 from 10:00 to 14:00 UTC. Compared to summer months, higher values of CO_2 are generally expected due to lower biosphere uptake

ACPD
11, 6875–6917, 2011

and shallower vertical mixing. Accumulation of CO_2 in the valley south of OXK was observed in the morning (10:30–11:30 UTC) between the aircraft's cumulative flown distance range 120 and 200 km (see Fig. 7a). CO_2 can accumulate in valleys under shallow vertical mixing in the nocturnal boundary layer as well as under nocturnal drainage conditions in complex terrain. The valley-mountain gradient in CO_2 concentrations in the valley decreased rapidly in the afternoon with the establishment of convective mixing and consequently enhanced vertical turbulence. STILT-VPRM and WRF-VPRM were able to capture relatively well the CO_2 accumulation in the valley in the morning (distance between 100 and 200 km); however WRF-VPRM slightly underestimated the vertical extent of valley accumulation during this period. At noon (distance between 280 and 320 km), STILT-VPRM overestimated the CO_2 concentrations and this overestimation can also be seen in the afternoon when the boundary layer is well mixed.

4 Discussion

4.1 Synoptic variability

The observations show considerable synoptic variability in CO_2 concentrations which are driven by atmospheric transport and surface flux heterogeneity. These synoptic variations in tracer concentrations provide valuable information on spatiotemporal patterns of surface fluxes and thus can be used in atmospheric inversion to construct regional fluxes. A synoptic event (cold front), observed on 18 August 2006, during which the observed CO_2 showed an enhancement of more than 20 ppm, is analyzed in detail to examine how such variations are represented by the mesoscale models. In the beginning of the event, the air temperature dropped significantly with a relatively sharp decrease in relative humidity (Fig. 3a–d). The wind speed was relatively high, reaching a maximum of 15 m s^{-1}. The atmospheric CO_2 observation shows a large peak during this period, which was captured by both models as seen in Figs. 6 and 8a,b. However the models predict this elevated concentration with a considerable low

ACPD
11, 6875–6917, 2011

bias of ~15 ppm. During the event, the air was coming from the south-west, and the time integrated footprints derived from STILT (sensitivity of mixing ratio at 07:00 UTC on 18 August to surface fluxes integrated over the past 48 h), shows a strong influence from the highly industrialized area in the south-west part of Germany occurring 10 h prior to the measurement (Fig. 8 c). Tracer simulations, where anthropogenic and biospheric contributions within the domain are separated, show a large contribution from respiration and emission fluxes for the event (Fig. 8a) and consequently an increase in CO_2 concentration in the atmosphere (Fig. 8b), which reached a peak in the early morning, owing to the shallow mixing in the nocturnal boundary layer. These higher concentrations started decreasing with the development of the convective mixed layer combined with the drawdown of CO_2 by photosynthesis. The above analysis suggests that OXK during this event was highly influenced by air carrying a large contribution from respiration, but also emissions originating from densely populated and industrialized area. The underestimation of the CO_2 peak in the models could be due to several reasons: (1) uncertainties in vertical mixing (this is the more likely scenario as it would strongly affect the vertical distribution of tracer concentrations, producing large model-data mismatches), (2) uncertainties in advection (WRF underestimated the wind speed in the beginning of the event and predicted south-easterly wind rather than the observed south-westerly wind direction. The strong south-westerly wind might be associated with advection of large plumes of CO_2 (respired and anthropogenic) to the measurement location), (3) the underestimation of anthropogenic emissions in the inventory for this area of influence (uncertainties of emission inventories at small spatial and short temporal scales can easily be as large as 50%, Olivier et al., 1999), (4) uncertainties in the VPRM respiration fluxes (note that VPRM simulates respiration fluxes as a linear function of the simulated surface temperature (at 2 m). The uncertainty due to a temperature bias is likely to be small because the simulated temperature for this period is fairly in good agreement with observations. However, the respiration fluxes in reality are not only controlled by temperature but also by other factors such as soil moisture), (5) underestimation of TM3 initial fields (it is more unlikely that a short term

ACPD
11, 6875–6917, 2011

event, which originated outside of Europe domain, would have had an influence on this). This emphasizes the complexities of mechanisms involved in such short-term scale events. The vertical profiling of CO_2 (as like DIMO aircraft campaign) or wind profiler measurements can be helpful to assess the impact of vertical mixing on tracer concentrations.

In general, both high-resolution models could capture the general trend of CO_2 variability during this synoptic event, by simulating well the influence of surface fluxes in the near-field and the atmosphere dynamics.

4.2 Orographic effect

The mountainous terrain can influence the regional circulation pattern around the tower site, resulting in local flow patterns which can have an impact on diurnal patterns in tracer concentration measurements. The local flow patterns are developed by the formation of (1) thermally forced mountain-valley circulations in response to radiative heating and cooling of the surface and (2) topographically induced stationary gravity waves (i.e., mountain waves) when stable flow encounters a mountain barrier. The downslope flows are more common at OXK during nighttime although mountain gravity waves are also likely in winter periods (based on WRF simulations as well as photographs taken during DIMO campaign).

4.2.1 Mountain-valley circulations

The mountain valley flows can change the atmospheric vertical mixing and can thus influence tracer measurements at OXK (Thompson et al., 2009). An example of such an event occurred at nighttime between 26 and 27 August 2006 is demonstrated in Fig. 9. During this period, the expected nocturnal CO_2 build up at OXK was found to be nearly absent owing to the thermally induced drainage flow. The data shown are the time series of meteorological and CO_2 observations at each level on the tower for a period from 26 to 28 August 2006. The period between the brown vertical dashed

ACPD
11, 6875–6917, 2011

lines in Fig. 9 shows evidence of mountain-valley circulation. Also the period was under weak synoptic pressure gradient conditions (as indicated by the simulated potential temperature) with a prevailing westerly flow (as indicated by the simulated wind speed) (Fig. 10a,c). The observed temperature and wind speed during this period (Fig. 9a,b) also suggest that the conditions were favorable for the formation of a buoyancy-driven downslope flow. Following radiative cooling of the surface on 26 August, relatively dry air intruded from the free troposphere into the nocturnal boundary layer, which was observed as a sharp decrease in the relative humidity (Fig. 9b). Noticeable time lags in the transition from moist to dry air were seen at the different sampling levels, which also indicate the intrusion of air from above. The evidence of dry air subsidence from the residual layer can also be seen later at 06:00 UTC on 27 August. Consequently, a decrease in CO_2 concentration was observed at 00:00 UTC and at 06:00 UTC on 27 August due to the replacement of air by the residual layer containing lower CO_2 concentration. STILT-VPRM captured well the lowering of CO_2 concentration at 06:00 UTC in response to the drainage flow and simulated well-mixed tracer concentrations in the nocturnal boundary layer. However WRF-VPRM showed an unrealistic accumulation of CO_2 concentration at the lower level which might be associated with the underestimation in the vertical extent of the entrainment air reaching the tower site. The presence of katabatic flow on the lee side of the mountain was predicted in WRF, indicated by the negative vertical velocity (downward movement of air) and increased wind speed along the mountain slope (Fig. 10d). The (simulated) impact of drainage flow on the tracer concentrations on the lee side of the mountain can be seen as a region of lower CO_2 contours in Fig. 10b.

4.2.2 Mountain wave activity

The buoyancy driven upslope and downslope flows, which are discussed above, are less common in winter due to low surface heating. As mentioned earlier, under stable stratified nocturnal boundary conditions, mountain gravity waves can be formed when air flow is perturbed with a barrier (e.g. mountain). Propagation of gravity waves

ACPD
11, 6875–6917, 2011

transporting mass and energy in the stable boundary layer can affect tracer concentrations measured at the tower. The possible occurrence of gravity waves can be assessed by estimating the Froude number (Stull, 1988), Fr (the ratio of inertial to gravitational forces, $= \frac{U}{(N \times h)}$) which relates the prevailing horizontal wind speed (U), mountain height (h) and buoyancy oscillation frequency (Brunt–Väisälä frequency, N – calculated as a function of potential temperature). When Fr is near unity, the wavelength of the air flow is in resonance with the mountain size, creating trapped mountain lee waves which results in strong downslope winds and enhanced turbulence on the lee side of the mountain.

However, the mountain wave activity is much more complex in reality and is difficult to interpret its effects on measurements. An ideal case of such an activity was occurred at a nighttime between 16 and 17 October 2006 (between brown dashed lines in Fig. 11). A temperature inversion was observed during this period (Fig. 11a) indicating the stable atmospheric conditions. The sharp decrease in observed relative humidity on the tower under relatively high wind speed indicates the presence of possible mountain wave activity with intrusion of dry air on the lee side of the mountain. These meteorological features were predicted reasonably well by the WRF model and the west-east cross section of simulated vertical velocity shows the downward movement of air at the lee side of the mountain (Fig. 12d). Note that the WRF simulations might not always capture the waves correctly and the caution has to be taken to interpret the structures of the vertical velocity fields which can also be formed due to the numerical noise. The increased gradient in the simulated potential temperature, together with higher values of simulated vertical velocity ($50\,\mathrm{cm\,s^{-1}}$) and strong wind speed, suggests the occurrence of mountain wave phenomena at the OXK site (Fig. 12). The Froude number was found to be close to unity, indicating the likelihood of gravity wave (mountain wave) activity. In addition to this, the simulated wavelengths λ ($= \frac{U}{N}$) for the region over the mountain were found to be close to the mountain height, showing the existence of vertically propagating mountain waves.

ACPD
11, 6875–6917, 2011

Following the collapse of the convective boundary layer on 16 October, CO_2 started to build up in the nocturnal shallow boundary layer and showed a distinctive gradient between layers for a few hours between 18:00–21:00 UTC. These nocturnal developments of CO_2 were captured fairly well in STILT-VPRM, however the vertical mixing between levels at 23 m and 90 m was underestimated. Corresponding to the prevailing mesoscale feature, the observed nocturnal gradient in tracer concentrations disappeared in response to the decent of air from the free troposphere. This was reproduced well in STILT-VPRM, while WRF-VPRM showed the decreasing tendency of CO_2 concentrations on this period but with an unrealistic gradient between the layers, which might be due to the underestimated mixing process. Note that vertical mixing is parameterized slightly differently in WRF-VPRM and STILT-VPRM. The influence of mountain waves on generating turbulent vertical mixing of nocturnal tracer concentrations at the lee side of the valley can be seen in the WRF-VPRM simulations (Fig. 12b). Owing to the strong downward movement of air and vertical mixing, a layer of lower CO_2 concentration was simulated for the western slope of the mountain, despite the nocturnal build-up period. The nocturnal build-up of CO_2 under shallow mixing and weak biological CO_2 uptake were simulated for the other valleys (Fig. 12b).

The above two case studies suggest that changes in the atmospheric transport and mixing in response to mesoscale phenomena, such as mountain-valley circulations and mountain wave activities, can strongly affect the diurnal patterns of CO_2 concentrations at OXK, and that these can be represented reasonably well in mesoscale models at the resolution of 2 km.

4.3 Seasonal variability

Different seasonal aspects, such as changes in thermal circulation patterns (changes in solar radiation), changes in diurnal patterns of vertical mixing, effects of snow cover and diurnal variations in surface fluxes, can have an important influence on measured tracer concentrations. Seasonal changes in the diurnal patterns of CO_2 concentration are observed at Ochsenkopf mountain station as it can be influenced by heterogeneous

ACPD
11, 6875–6917, 2011

land sources and sinks as well as by synoptic atmospheric conditions. Figure 13 shows averaged diurnal cycles of observed and modeled CO_2 at different measurement levels and for different seasons. Except for the level 163 m in winter and autumn, the CO_2 concentration maxima were observed during nighttime due to the accumulation of CO_2 concentration in the shallow nocturnal boundary layer. The measurement level at 163 m during winter and autumn is more representative of free tropospheric or residual layer air, as indicated by the weak diurnal changes in observed concentrations and by the decoupling relative to the lower levels. The slight daytime increase at the 163 m level, delayed by about six hours compared to the lower levels, is consistent with the daytime mixing of air previously trapped in the stable mixed layer, containing remnants of respired CO_2 from the previous night. The amplitude of the diurnal cycle is larger in spring and summer months ($\sim$ 8 ppm), consistent with the enhanced biospheric activity (photosynthesis and ecosystem respiration), whereas the amplitude is smaller in autumn and winter months owing to the reduced diurnal variability in the terrestrial fluxes. The low values of CO_2 are noticeable in August (active growing season) due to enhanced biospheric CO_2 uptake. The model-data agreement is fairly good for higher resolution models, except for the level 163 m in winter and autumn seasons where both models overestimate the vertical mixing. The coarse resolution TM3 analyzed CO_2 fields (taken from 940 hectopascal (hPa) TM3 pressure level which corresponds to the measurement levels above sea level, i.e. relative to the sea level; indicated as "TM3" in Fig. 13) show little diurnal change during all seasons and at all levels. On the other hand, TM3 analyzed CO_2 fields corresponding to the model levels close to the measurement levels from the surface, i.e. relative to the model terrain (taken from 1013 hPa and 1002 hPa TM3 pressure levels corresponding to the levels on the tower; indicated as "TM3-surface" in Fig. 13) show large diurnal variability due to the strong influence of surface fluxes near the ground, but with large positive biases in most of the cases. This discrepancy can lead to potential biases in flux estimates when using measurements from a site like OXK, as discussed above. Again, this suggests the importance of using high-resolution models to resolve the large variability of atmospheric

ACPD
11, 6875–6917, 2011

CO_2 concentrations in response to variability in surface fluxes and mesoscale transport. In order to examine whether the poor performances of TM3 are caused by the coarse resolution flux fields (horizontal resolution: $4^\circ \times 5^\circ$), we run STILT-VPRM with biospheric fluxes aggregated to ~500 km × 500 km resolution, comparable to the TM3 resolution. CO_2 simulated by this coarse resolution version of STILT-VPRM shows remarkable similarity to the high-resolution simulations by STILT and WRF in the diurnal cycle for the different seasons.

4.4 Vertical distribution of CO_2 concentrations

The vertical profiling of atmospheric CO_2 during aircraft campaigns provides more information on vertical mixing in the atmosphere and provide the opportunity to evaluate current transport models. The discrepancies in predicting atmospheric mixing can lead to a strong bias in the simulated vertical distribution of CO_2 concentrations. An example of such an effect can be seen in Figs. 5 and 7. The underestimation of the vertical extent of CO_2 accumulation (as mentioned in Sect. 3.2.2, Fig. 11a,b) can be caused by the overestimation of vertical mixing in WRF. The effect of this overestimation can also be seen in the modeled specific humidity (Fig. 5b) as low values (underestimation) in the upper layers. Note that the wind speed was predicted well in WRF with negligible bias.

It should also be mentioned that the difference in observed and modeled wind speed found at the Ochsenkopf valley for another day of the campaign (23 October 2008) generated an underestimation of CO_2 concentration in both WRF-VPRM and STILT-VPRM (figure not shown). WRF underestimated the flow of air, advected from upstream locations and consequently failed to capture the huge contribution of the advected respired signal to the measurement locations. STILT-VPRM also shows a similar underestimation of CO_2 concentration for the same reason.

These two case studies of model evaluation with the airborne measurements show the necessity of accurately predicting the mesoscale atmospheric transport, such as advection and convection, as well as vertical mixing. Both models are able to capture

ACPD
11, 6875–6917, 2011

the spatial variability of measured CO_2 concentration in the complex terrain for most of the cases and the discrepancy between models and measurements are mainly attributed to the difference in representing atmospheric PBL dynamics.

5 Summary and conclusions

High-resolution modeling simulations of meteorological fields and atmospheric CO_2 concentrations, provided by WRF-VPRM and STILT-VPRM, are presented together with measurements obtained from the Ochsenkopf tower (OXK) and from an aircraft campaign, to address the representativeness of greenhouse gas measurements over a complex terrain associated with surrounding mountain ranges. The spatial and temporal patterns of CO_2 are reproduced remarkably well in high-resolution models for different seasons when compared to the coarse model (TM3). This emphasizes the importance of using high-resolution modeling tools in inverse frameworks, since a small deviation in CO_2 concentration can lead to potentially large biases in flux estimates. The actual reduction in uncertainties of flux estimates when using high-resolution models (compared to lower-resolution models) in the inverse framework needs to be further investigated.

The measurements of CO_2 at OXK show diurnal, synoptic and seasonal variability of CO_2 due to different aspects such as changes in the diurnal patterns of vertical mixing, diurnal variations in surface fluxes, effect of front passage, changes in thermal circulation patterns etc. These variations in tracer concentrations provide valuable information on spatiotemporal patterns of surface fluxes and thus can be used in atmospheric inversions to construct regional fluxes. Both high-resolution models were able to capture this variability by simulating well the influence of surface fluxes in the near-field and the atmosphere dynamics.

The mesoscale flows, such as mountain wave activity and mountain-valley circulations, can have a strong influence on the observed atmospheric CO_2 at OXK by changing the vertical mixing of the tracer concentrations. The meteorological simulations by

ACPD
11, 6875–6917, 2011

WRF indicate that the buoyancy driven drainage flows are more common at OXK during nighttimes (especially in summer) and mountain gravity waves are likely to occur in winter periods. Resolving these circulation patterns in models is a prerequisite for utilizing observations from mountain stations such as OXK with a reduced representation error.

The discrepancies in predicting vertical mixing can lead to strong biases in simulated CO_2 concentrations and these kinds of uncertainties are typical for complex terrain regions. The vertical profiling of CO_2 (like the DIMO aircraft campaign) or wind profiler measurements can be helpful in assessing the impact of vertical mixing on tracer concentrations. Our study shows that much of the variability in CO_2 concentrations can be reproduced well by appropriate representation of mesoscale transport processes, such as advection, convection and vertical mixing as well as surface flux influences in the near-field.

This study demonstrates the potential of using high-resolution models in the context of inverse modeling frameworks to utilize measurements provided from mountain or complex terrain sites. Our future work will focus on regional inversions using STILT-VPRM at high-resolution with a nested option. The feasibility of using these high-resolution nests in global models has already been demonstrated by (Rödenbeck et al., 2009). This provides justified hope that measurements from mountain stations can be utilized in inverse modeling frameworks to derive regional CO_2 budgets at reduced uncertainty limits.

Acknowledgement. We thank Prof. Dr. Martin Heimann, Max Planck Institute of Biogeochemistry, Germany for continuing support and helpful discussions. We thank Thomas Foken, University of Bayreuth, Germany for providing wind profiler data. We are also thankful to the whole Ochsenkopf tall tower team in Max Planck Institute of Biogeochemistry, Germany for their assistance in data processing.

The service charges for this open access publication
have been covered by the Max Planck Society.

ACPD
11, 6875–6917, 2011

References

Ahmadov, R., Gerbig, C., Kretschmer, R., Koerner, S., Neininger, B., Dolman, A. J., and Sarrat, C.: Mesoscale covariance of transport and CO_2 fluxes: Evidence from observations and simulations using the WRF-VPRM coupled atmosphere-biosphere model, J. Geophys. Res.-Atmos., 112, D22107, doi:10.1029/2007JD008552, 2007.

Ahmadov, R., Gerbig, C., Kretschmer, R., Körner, S., Rödenbeck, C., Bousquet, P., and Ramonet, M.: Comparing high resolution WRF-VPRM simulations and two global CO_2 transport models with coastal tower measurements of CO_2, Biogeosciences, 6, 807–817, doi:10.5194/bg-6-807-2009, 2009.

Denning, A. S., Zhang, N., Yi, C. X., Branson, M., Davis, K., Kleist, J., and Bakwin, P.: Evaluation of modeled atmospheric boundary layer depth at the WLEF tower, Agr. Forest Meteorol., 148, 206–215, 2008.

Enting, I. G.: Inverse problems in atmospheric constituent studies: III. Estimating errors in surface sources, Inverse Probl., 9, 649–665, 1993.

Gangoiti, G., Millan, M. M., Salvador, R., and Mantilla, E.: Long-range transport and recirculation of pollutants in the Western Mediterranean during the project Regional Cycles of Air Pollution in the West-Central Mediterranean area, Atmos. Environ., 35(36), 6267–6276, 2001.

Geels, C., Gloor, M., Ciais, P., Bousquet, P., Peylin, P., Vermeulen, A. T., Dargaville, R., Aalto, T., Brandt, J., Christensen, J. H., Frohn, L. M., Haszpra, L., Karstens, U., Rödenbeck, C., Ramonet, M., Carboni, G., and Santaguida, R.: Comparing atmospheric transport models for future regional inversions over Europe – Part 1: mapping the atmospheric CO_2 signals, Atmos. Chem. Phys., 7, 3461–3479, doi:10.5194/acp-7-3461-2007, 2007.

Gerbig, C., Körner, S., and Lin, J. C.: Vertical mixing in atmospheric tracer transport models: error characterization and propagation, Atmos. Chem. Phys., 8, 591–602, doi:10.5194/acp-8-591-2008, 2008.

Gerbig, C., Dolman, A. J., and Heimann, M.: On observational and modelling strategies targeted at regional carbon exchange over continents, Biogeosciences, 6, 1949–1959, doi:10.5194/bg-6-1949-2009, 2009.

Gourdji, S. M., Mueller, K. L., Schaefer, K., and Michalak, A. M.: Global monthly averaged CO_2 fluxes recovered using a geostatistical inverse modeling approach: 2. Results including auxiliary environmental data, J. Geophys. Res.-Atmos., 113, D21115,

ACPD
11, 6875–6917, 2011

doi:10.1029/2007JD009733, 2008.
Gurney, K. R., Law, R. M., Denning, A. S., Rayner, P. J., Baker, D., Bousquet, P., Bruhwiler, L., Chen, Y.-H., Ciais, P., Fan, S., Fung, I. Y., Gloor, M., Heimann, M., Higuchi, K., John, J., Maki, T., Maksyutov, S., Masarie, K., Peylin, P., Prather, M., Pak, B. C., Randerson, J., Sarmiento, J., Taguchi, S., Takahashi, T., and Yuen, C.-W.: Towards robust regional estimates of CO_2 sources and sinks using atmospheric transport models, Nature, 415, 626–630, 2002.
Heimann, M. and Koerner, S.: The global atmospheric tracer model TM3, Technical Reports, Max-Planck-Institute for Biogeochemie, 5, 131 pp., 2003.
Jacobson, A. R., Mikaloff Fletcher, S. E., Gruber, N., Sarmiento, J. L., and Gloor, M.: A joint atmosphere-ocean inversion for surface fluxes of carbon dioxide: 1. Methods and global-scale fluxes, Global Biogeochem. Cy., 21, GB1019, doi:10.1029/2005GB002556, 2007.
Lauvaux, T., Uliasz, M., Sarrat, C., Chevallier, F., Bousquet, P., Lac, C., Davis, K. J., Ciais, P., Denning, A. S., and Rayner, P. J.: Mesoscale inversion: first results from the CERES campaign with synthetic data, Atmos. Chem. Phys., 8, 3459–3471, doi:10.5194/acp-8-3459-2008, 2008.
Le Treut, H., Somerville, R., Cubasch, U., Ding, Y., Mauritzen, C., Mokssit, A., Peterson, T., and Prather, M.: Historical Overview of Climate Change, In: Climate Change 2007: The Physical Science Basis. Contribution of Working Group I to the Fourth Assessment Report of the Intergovernmental Panel on Climate Change, edited by: Solomon, S., Qin, D., Manning, M., Chen, Z., Marquis, M., Averyt, K. B., Tignor, M., and Miller, H. L., Cambridge University Press, Cambridge, UK and New York, NY, USA, 2007.
Levin, I., Graul, R., and Trivett, N.: Long-term observations of atmospheric CO_2 and carbon isotopes at continental sites in Germany, Tellus B, 47, 23–34, 1995.
Lin, J. C. and Gerbig, C.: Accounting for the effect of transport errors on tracer inversions, Geophys. Res. Lett., 32, L01802, doi:10.1029/2004GL021127, 2005.
Lin, J. C., Gerbig, C., Wofsy, S. C., Andrews, A. E., Daube, B. C., Davis, K. J., and Grainger, C. A.: A near-field tool for simulating the upstream influence of atmospheric observations: The stochastic time-inverted Lagrangian transport (STILT) model, J. Geophys. Res.-Atmos., 108, 4493, doi:10.1029/2002JD003161, 2003.
Mahadevan, P., Wofsy, S. C., Matross, D. M., Xiao, X., Dunn, A. L., Lin, J. C., Gerbig, C., Munger, J. W., Chow, V. Y., and Gottlieb, E. W.: A satellite-based biosphere parameterization for net ecosystem CO_2 exchange: vegetation photosynthesis and respiration model (VPRM),

ACPD
11, 6875–6917, 2011

Global Biogeochem. Cy., 22, GB2005, doi:10.1029/2006GB002735, 2008.
Matross, D. M., Andrews, A., Pathmathevan, M., Gerbig, C., Lin, J. C., Wofsy, S. C., Daube, B. C., Gottlieb, E. W., Chow, V. Y., Lee, J. T., Zhao, C. L., Bakwin, P. S., Munger, J. W., and Hollinger, D. Y.: Estimating regional carbon exchange in New England and Quebec by combining atmospheric, ground-based and satellite data, Tellus B, 58, 344–358, 2006.
Nehrkorn, T., Eluszkiewicz, J., Wofsy, S. C., Lin, J. C., Gerbig, C., Longo, M., and Freitas, S.: Coupled weather research and forecasting–stochastic time-inverted lagrangian transport (WRF–STILT) model, Meteorol. Atmos. Phys., 107, 51–64, 2010.
Olivier, J. G. J., Bouwman, A. F., Berdowski, J. J. M., Veldt, C., Bloos, J. P. J., Visschedijk, A. J. H., and van der Maas, C. W. M.: Sectoral emission inventories of greenhouse gases for 1990 on a per country basis as well as on $1^{\circ} \times 1^{\circ}$, Environ. Sci. Policy, 2, 241–263, 1999.
Pérez-Landa, G., Ciais, P., Gangoiti, G., Palau, J. L., Carrara, A., Gioli, B., Miglietta, F., Schumacher, M., Millán, M. M., and Sanz, M. J.: Mesoscale circulations over complex terrain in the Valencia coastal region, Spain – Part 2: Modeling CO_2 transport using idealized surface fluxes, Atmos. Chem. Phys., 7, 1851–1868, doi:10.5194/acp-7-1851-2007, 2007.
Peters, W.: Seven years of recent European net terrestrial carbon dioxide exchange constrained by atmospheric observations, Glob. Change Biol., 16, 1317–1337, 2010.
Pillai, D., Gerbig, C., Kretschmer, R., Beck, V., Karstens, U., and Neininger, B.: Comparing Lagrangian and Eulerian models for CO_2 transport – a step towards Bayesian Inverse Modeling using WRF/STILT-VPRM, in preparation, 2011.
Pillai, D., Gerbig, C., Marshall, J., Ahmadov, R., Kretschmer, R., Koch, T., and Karstens, U.: High resolution modeling of CO_2 over Europe: implications for representation errors of satellite retrievals, Atmos. Chem. Phys., 10, 83–94, doi:10.5194/acp-10-83-2010, 2010.
Reiter, R., Sladkovic, R., and Kanter, H. J.: Concentration of trace gases in the lower troposphere, Part I: Carbon dioxide, Meteorol. Atmos. Phys., 35, 187–200, 1986.
Rödenbeck, C.: Estimating CO_2 sources and sinks from atmospheric mixing ratio measurements using a global inversion of atmospheric transport. Technical Report 6, Max-Planck Institut für Biogeochemie, Jena, Germany, 53 pp., 2005.
Rödenbeck, C., Houweling, S., Gloor, M., and Heimann, M.: CO_2 flux history 1982–2001 inferred from atmospheric data using a global inversion of atmospheric transport, Atmos. Chem. Phys., 3, 1919–1964, doi:10.5194/acp-3-1919-2003, 2003.
Rödenbeck, C., Gerbig, C., Trusilova, K., and Heimann, M.: A two-step scheme for high-

ACPD
11, 6875–6917, 2011

resolution regional atmospheric trace gas inversions based on independent models, Atmos. Chem. Phys., 9, 5331–5342, doi:10.5194/acp-9-5331-2009, 2009.

Sarrat, C., Noilhan, J., Lacarrère, P., Donier, S., Lac, C., Calvet, J. C., Dolman, A. J., Gerbig, C., Neininger, B., Ciais, P., Paris, J. D., Boumard, F., Ramonet, M., and Butet, A.: Atmospheric CO_2 modeling at the regional scale: application to the CarboEurope regional experiment, J. Geophys. Res.-Atmos., 112, D12105, doi:10.1029/2006JD008107, 2007.

Stull, R. B.: An Introduction to Boundary Layer Meteorology, Kluwer Academic Publishers, Dordrecht, 666 pp., 1988.

Tans, P. P., Fung, I. Y., and Takahashi, T.: Observational constraints on the global atmospheric CO_2 budget, Science, 247, 1431–1438, 1990.

Thompson, R. L., Manning, A. C., Gloor, E., Schultz, U., Seifert, T., Hänsel, F., Jordan, A., and Heimann, M.: In-situ measurements of oxygen, carbon monoxide and greenhouse gases from Ochsenkopf tall tower in Germany, Atmos. Meas. Tech., 2, 573–591, doi:10.5194/amt-2-573-2009, 2009.

Tolk, L. F., Meesters, A. G. C. A., Dolman, A. J., and Peters, W.: Modelling representation errors of atmospheric CO_2 mixing ratios at a regional scale, Atmos. Chem. Phys., 8, 6587–6596, doi:10.5194/acp-8-6587-2008, 2008.

van der Molen, M. K. and Dolman, A. J.: Regional carbon fluxes and the effect of topography on the variability of atmospheric CO_2, J. Geophys. Res.-Atmos., 112, D01104, doi:10.1029/2006JD007649, 2007.

ACPD
11, 6875–6917, 2011

Table 1. Summary statistics of observed and simulated (WRF) meteorological fields (model bias (bias), standard deviation (sd) and squared correlation coefficient (R^2)) using hourly time series at available measurement levels for different seasons.

Season	Level	Temperature			Relative humidity			u-Component			v-Component		
		bias	sd	R^2	bias	sd	R^2	bias	sd	R^2	bias	sd	R^2
Spring	163	1.2	1.4	0.81	2.8	9.8	0.84	0.9	3.1	0.92	1.2	2.3	0.66
(May 2006)	90	0.7	1.3	0.80	0.4	10.9	0.71	–	–	–	–	–	–
Summer	163	1.3	1.0	0.86	−0.2	6.7	0.74	0.3	2.7	0.70	1.1	2.7	0.61
(Aug 2006)	90	0.8	1.1	0.86	−4.7	8.3	0.60	–	–	–	–	–	–
Autumn	163	0.2	1.7	0.68	6.2	14.0	0.79	2.2	3.4	0.81	0.2	3.0	0.65
(Oct 2006)	90	−0.1	1.6	0.67	3.8	14.7	0.62	–	–	–	–	–	–
Winter	163	1.4	0.9	0.93	−1.9	9.0	0.52	0.6	6.4	0.48	1.2	5.0	0.33
(Mar 2008)	90	1.2	1.0	0.91	−6.4	12.2	0.48	–	–	–	–	–	–

ACPD
11, 6875–6917, 2011

Table 2. Summary statistics of observed and simulated CO_2 fields (model bias (bias), standard deviation (sd) and squared correlation coefficient (R^2)) using 3-h time series at available measurement levels for different seasons. Simulated fields are provided by TM3, STILT-VPRM and WRF-VPRM.

Season	Level	TM3			STILT-VPRM			WRF-VPRM		
		bias	sd	R^2	bias	sd	R^2	bias	sd	R^2
Spring	163	−1.9	3.1	0.11	−1.7	3.0	0.33	1.4	2.7	0.41
(May 2006)	90	−1.7	3.2	0.16	−1.7	2.8	0.50	1.4	2.4	0.57
	23	−1.1	4.1	0.09	−1.6	2.8	0.58	1.6	2.8	0.58
Summer	163	0.5	4.0	0.01	0.6	2.8	0.50	0.8	2.9	0.46
(Aug 2006)	90	0.4	4.8	0.02	0.3	3.2	0.58	0.6	3.3	0.55
	23	0.8	5.0	0.01	−0.1	3.4	0.52	0.5	3.1	0.62
Autumn	163	2.6	3.9	0.39	−0.5	3.1	0.59	0.6	3.3	0.51
(Oct 2006)	90	3.4	4.7	0.29	−0.4	3.4	0.62	0.6	3.9	0.52
	23	4.6	5.5	0.21	−0.4	4.4	0.52	0.3	4.7	0.49
Winter	163	1.6	2.1	0.17	−0.5	2.2	0.20	0.5	2.3	0.23
(Mar 2008)	90	1.5	2.1	0.19	−0.8	1.8	0.42	0.4	2.2	0.30
	23	2.1	2.6	0.14	−0.8	2.4	0.37	0.5	2.6	0.32

ACPD
11, 6875–6917, 2011

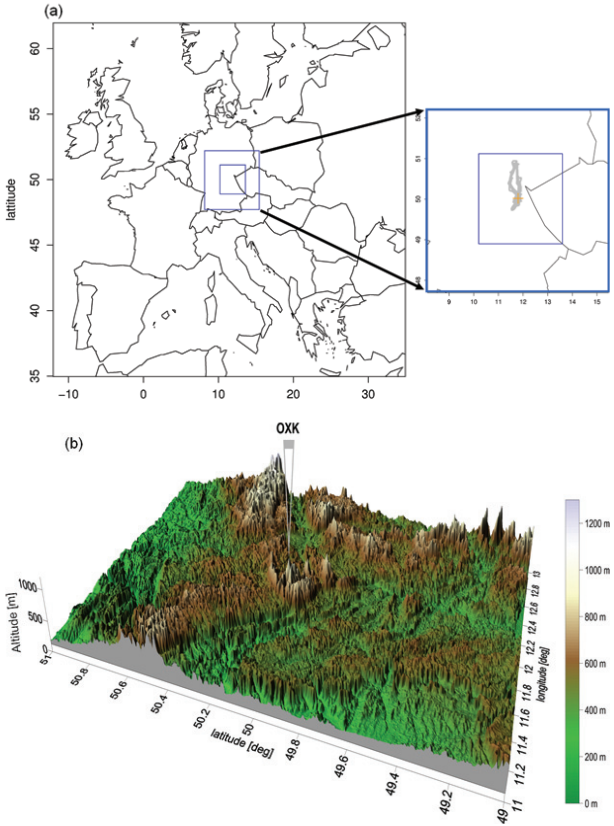

Fig. 1. **(a)** Map showing model domains used for WRF and STILT. STILT uses the larger domain covering Europe with two nests indicated by the blue rectangles. These two rectangles in blue represent the WRF domains, which are centered over OXK (50°01′ N, 11°48′ E, marked with "+"). A zoom of the WRF domain is showed in right-hand side of the main figure with an example of a DIMO flight track overlaid in grey lines. **(b)** Topography around OXK (the color gradient shows terrain height above sea-level).

ACPD
11, 6875–6917, 2011

High-resolution simulations of atmospheric CO_2 over complex terrain

D. Pillai et al.

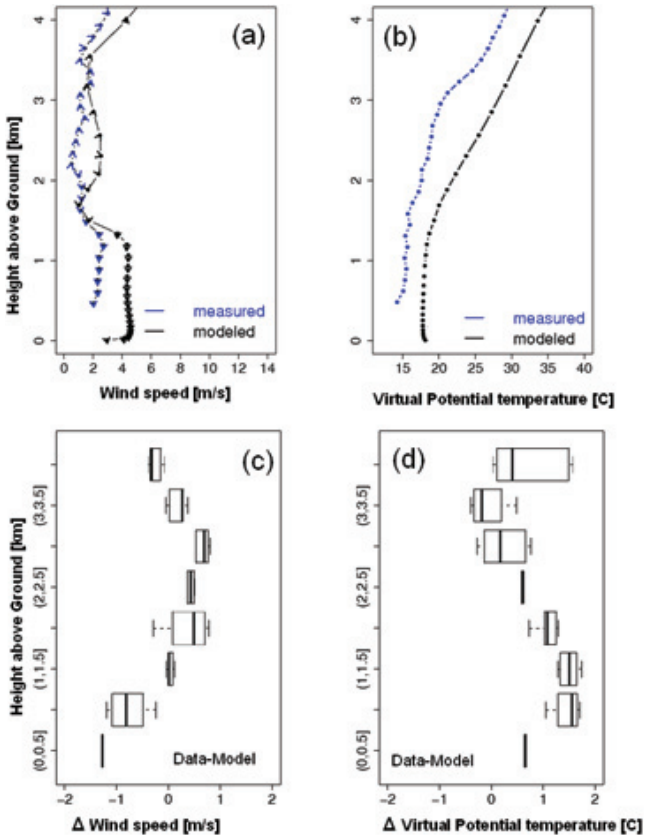

Fig. 2. **(a,b)** Profiles of observed vs. modeled wind fields and virtual potential temperature for 3 August 2006 at 15:00 UTC. The horizontal direction of wind is indicated with arrowheads **(c,d)** the data-model mismatch for the monthly averages of these fields at 15:00 UTC, plotted against different altitude bins. The box indicates 95% quartile, the whisker denotes minimum and maximum of deviations and the vertical bar inside the box denotes the median.

ACPD
11, 6875–6917, 2011

High-resolution simulations of atmospheric CO_2 over complex terrain

D. Pillai et al.

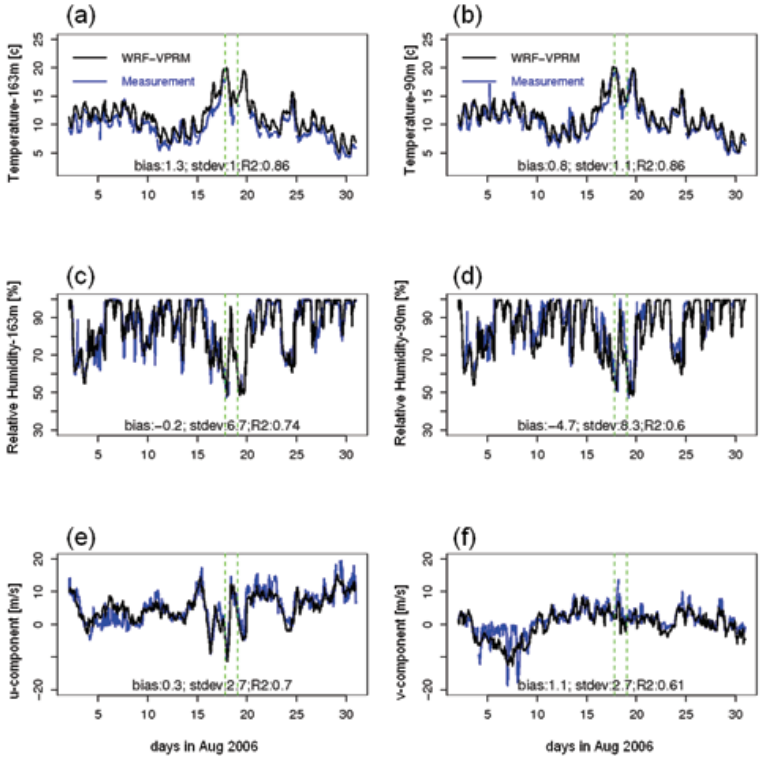

Fig. 3. Comparison of measured and modeled meteorological parameters for August 2006 at the OXK site: **(a,b)** temperature at 163 m and 90 m, **(c,d)** relative humidity at 163 m and 90 m, and **(e,f)** horizontal components of wind at 163 m. The green dotted vertical lines denotes the passage of a cold front investigated in detail (see Sect. 4.1). The summary statistics of observed and simulated fields – data-model bias, standard deviation of data-model differences and squared correlation coefficient – are given inside each panel.

ACPD
11, 6875–6917, 2011

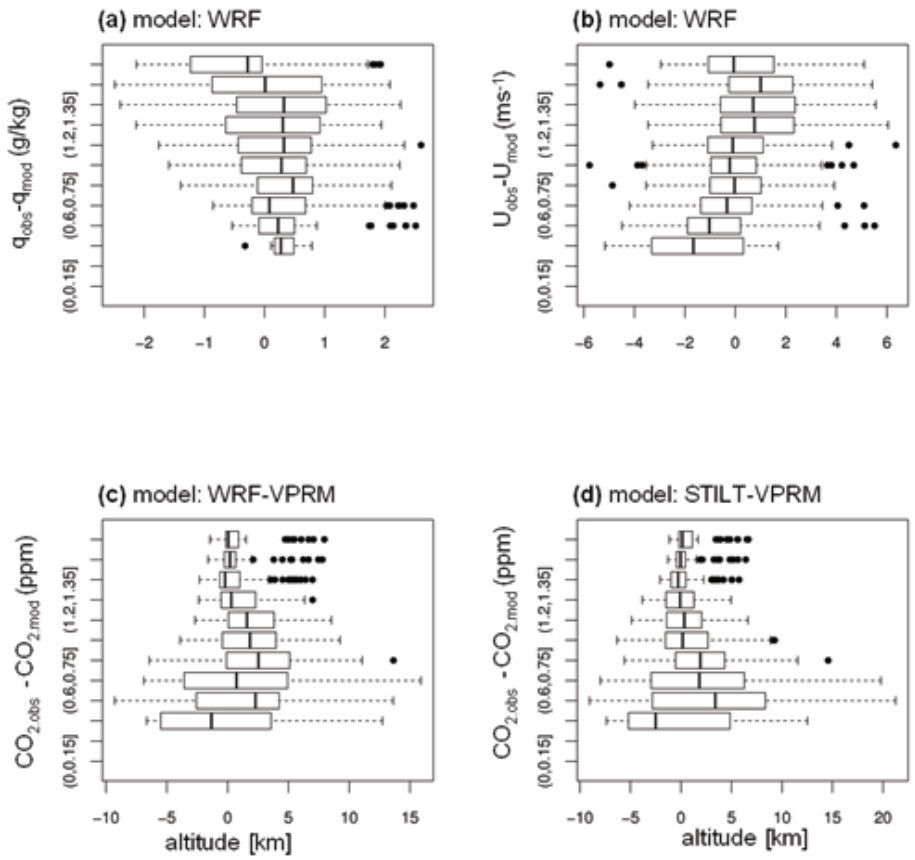

Fig. 4. The box-whisker plot of model mismatch (observations-simulations) using all aircraft profiles for **(a)** specific humidity, **(b)** wind speed, and **(c)** CO_2 (WRF-VPRM), **(d)** CO_2 (STILT-VPRM).The box indicates 95% quartile, the whisker denotes minimum and maximum of deviations and the vertical bar inside the box denotes the median. Black dots are outliers.

ACPD
11, 6875–6917, 2011

High-resolution simulations of atmospheric CO_2 over complex terrain

D. Pillai et al.

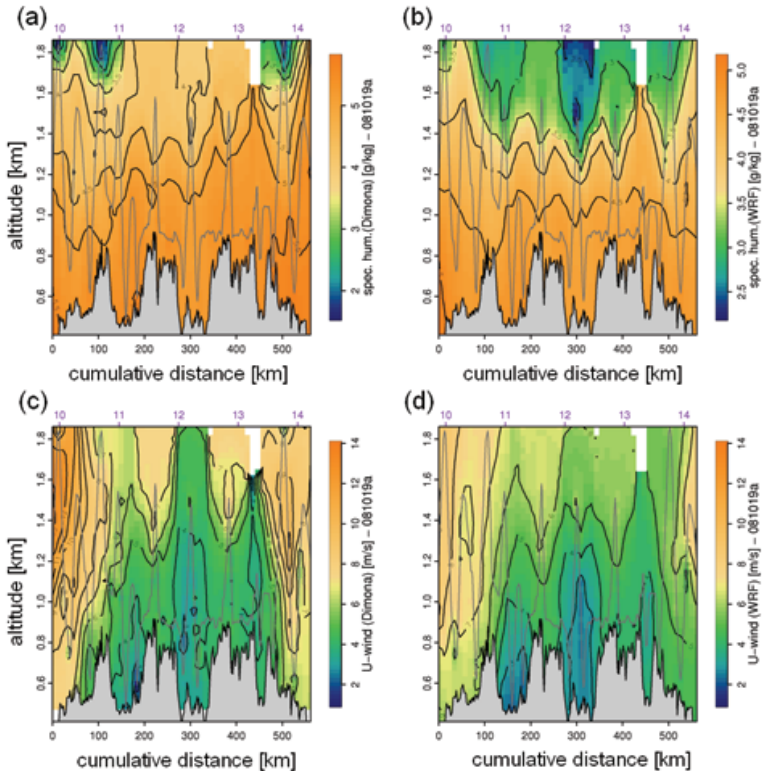

Fig. 5. Vertical cross section (using a distance weighted interpolation) of the observed and simulated meteorological fields as a function of distance flown by the aircraft for 19 October 2006: **(a,b)** specific humidity in $g\,kg^{-1}$, **(c,d)** wind speed in $m\,s^{-1}$. **(a)** and **(c)** represent measurements, and **(b)** and **(d)** represent WRF simulations. The grey lines indicate flight track and the shaded grey region represents terrain elevation. See Fig. 7d for aircraft track showing altitude above ground. Time of the measurements/simulations is given in the top X-axis.

ACPD
11, 6875–6917, 2011

High-resolution simulations of atmospheric CO_2 over complex terrain

D. Pillai et al.

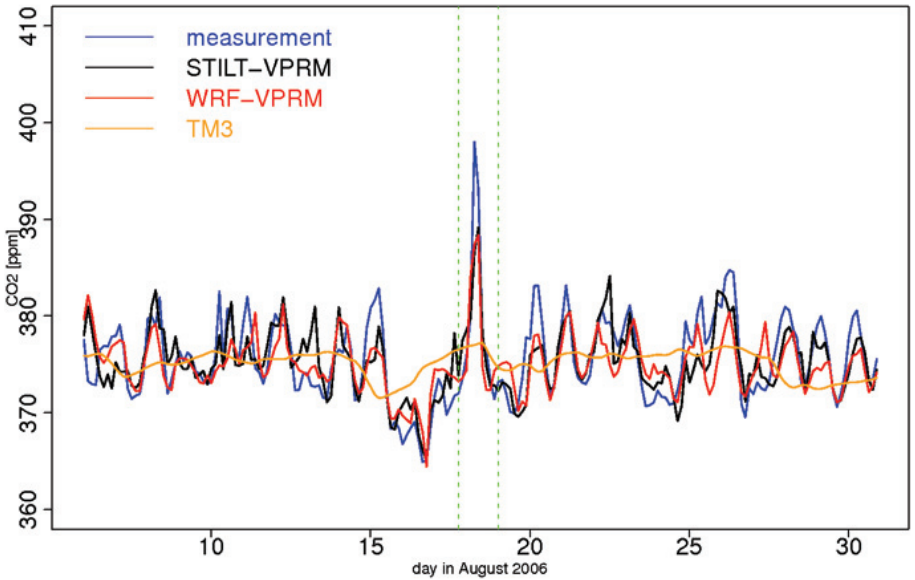

Fig. 6. Comparison of measured and modeled CO_2 concentrations for August 2006 at 90 m on the OXK. A period between dashed green vertical bars denotes a synoptic event during 00:00 to 15:00 UTC on 18 August 2006 (see also Sect. 4.1).

ACPD
11, 6875–6917, 2011

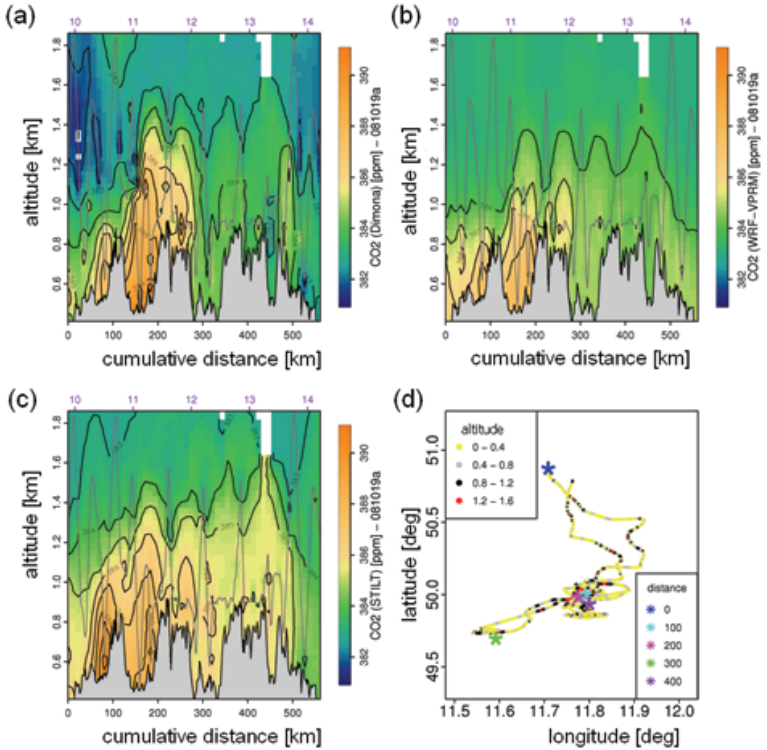

Fig. 7. Vertical cross section (using a distance weighted interpolation) of the observed and simulated CO_2 fields (given in ppm) as a function of distance flown by the aircraft (cumulative distance) for 19 October 2006: **(a)** measurements, **(b)** WRF-VPRM, **(c)** STILT-VPRM, and **(d)** flight track with color gradient showing altitude range (legend at the top left-hand side of the panel) above ground. The symbol "*" denotes cumulative distance in km (legend at the bottom right-hand side of the panel). In **(a–c)**, the time of measurements/simulations is given in the top *X*-axis.

ACPD
11, 6875–6917, 2011

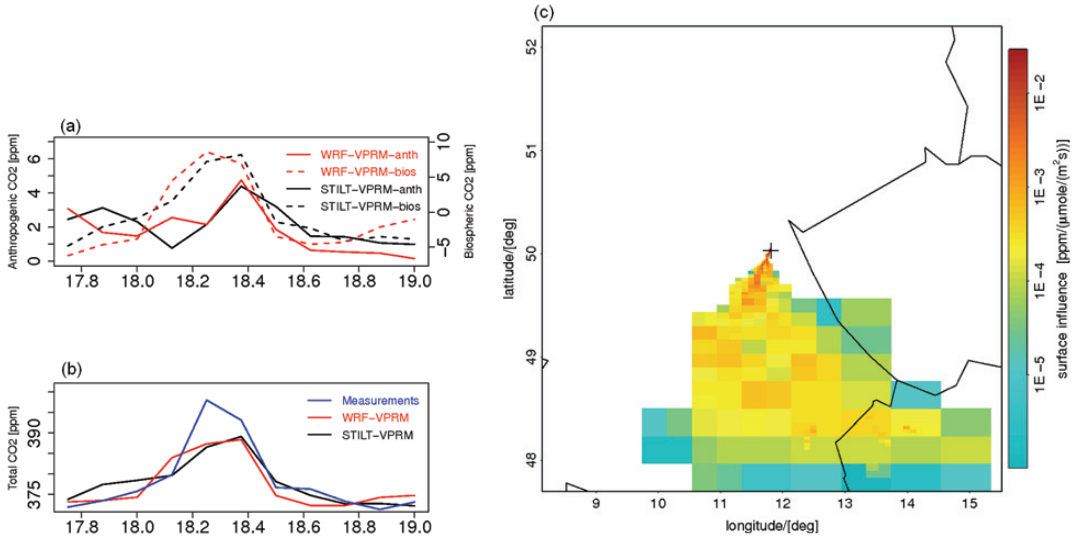

Fig. 8. Influence of surface fluxes on measured CO_2 concentration at OXK: **(a)** and **(b)** time series of simulated anthropogenic and biospheric CO_2 signals (contribution of anthropogenic and biospheric fluxes to the total CO_2) at 90 m on the tower during 17–18 August 2006. **(c)** Time integrated footprints derived by STILT on 18 August 2006 at 07:00 UTC for particles running −48 h (backward in time) from tower (indicated with + sign).

ACPD
11, 6875–6917, 2011

High-resolution simulations of atmospheric CO_2 over complex terrain

D. Pillai et al.

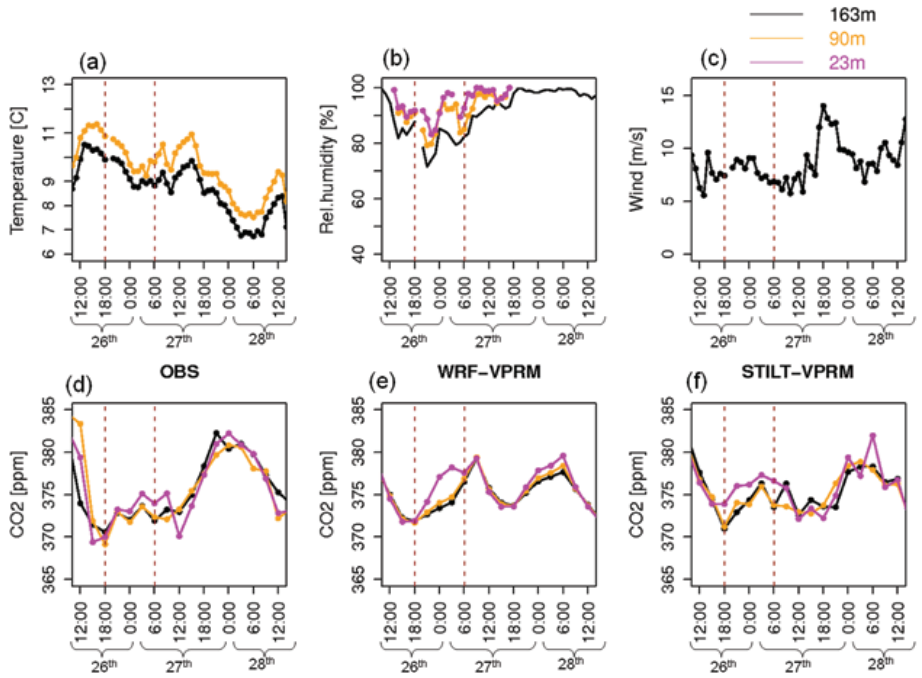

Fig. 9. Time series of meteorological parameters and CO_2 concentrations for different levels at OXK site during 26–28 August 2006: **(a–c)** observed air-temperature, relative humidity and wind speed, respectively, **(d–f)** CO_2 concentration, observed and modeled by WRF and STILT, respectively. The area between dashed brown vertical bars denotes the period under mountain-valley circulation. The *X*-axis shows hours in UTC; the horizontal extent of curly bracket at the bottom of *X*-axis shows the day on August 2006.

ACPD
11, 6875–6917, 2011

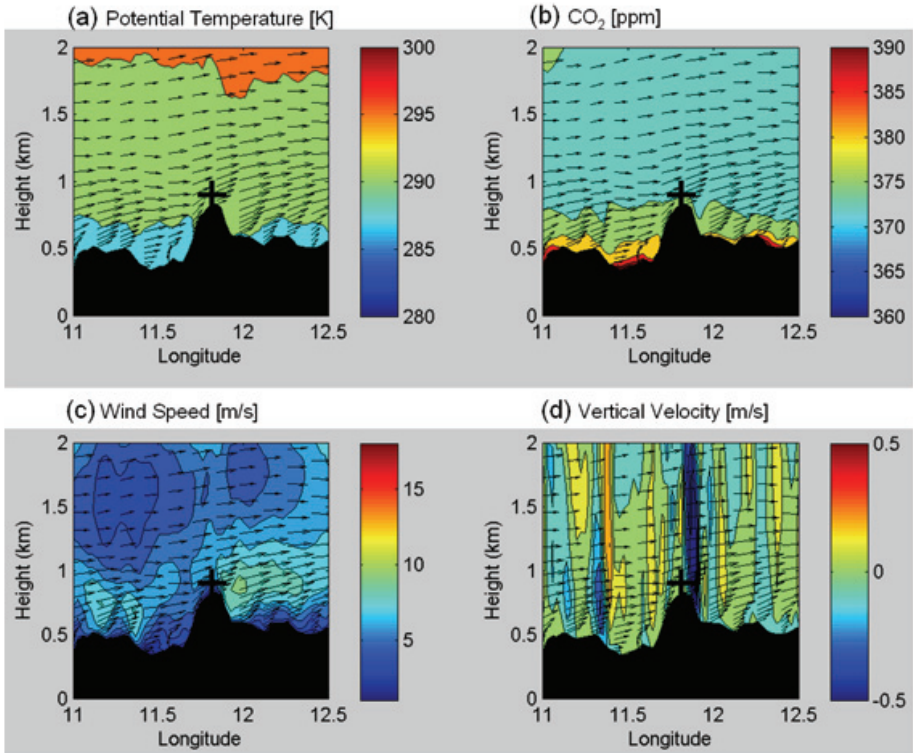

Fig. 10. Vertical cross section along OXK latitude (50°01′ N) on 27 August 2006 at 01:00 UTC, showing WRF-VPRM simulated **(a)** potential temperature in Kelvin, **(b)** CO_2 concentration in ppm, **(c)** wind speed in $m\,s^{-1}$, and **(d)** vertical velocity in $m\,s^{-1}$. The overlaid arrows indicate prevailed wind direction; the symbol "+" indicates OXK location.

ACPD
11, 6875–6917, 2011

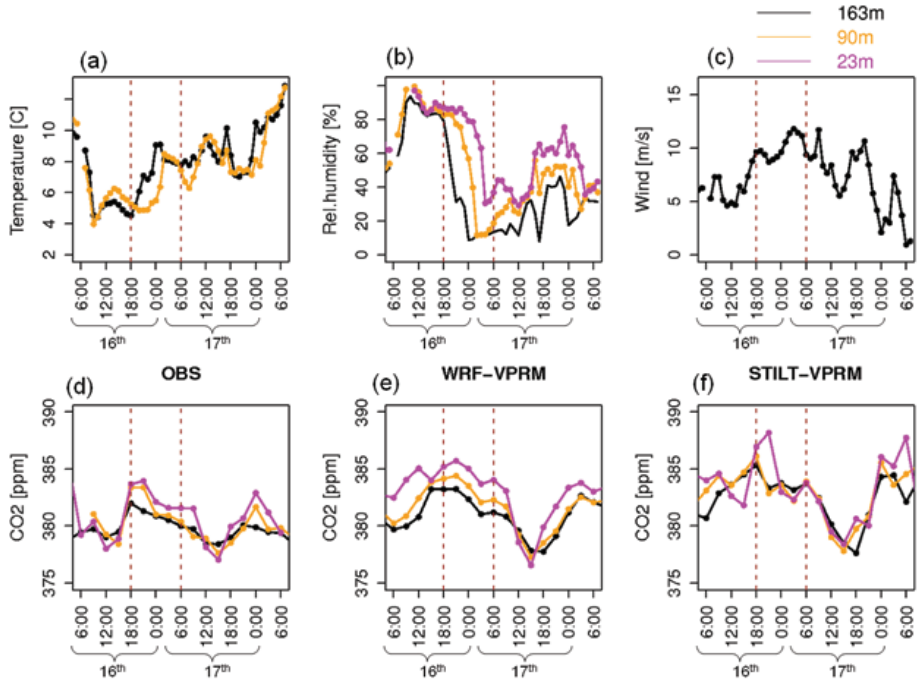

Fig. 11. Time series of meteorological parameters and CO_2 concentrations for different levels at Ochsenkopf tower site during 16–17 October 2006: **(a–c)** observed air-temperature, relative humidity and wind speed, respectively, **(d–f)** CO_2 concentration-observed, modeled by WRF and STILT, respectively. The area between dashed brown vertical bars denotes the period under mountain wave activity. The *X*-axis shows hours in UTC; the horizontal extent of curly bracket at the bottom of *X*-axis shows the day on October 2006.

ACPD
11, 6875–6917, 2011

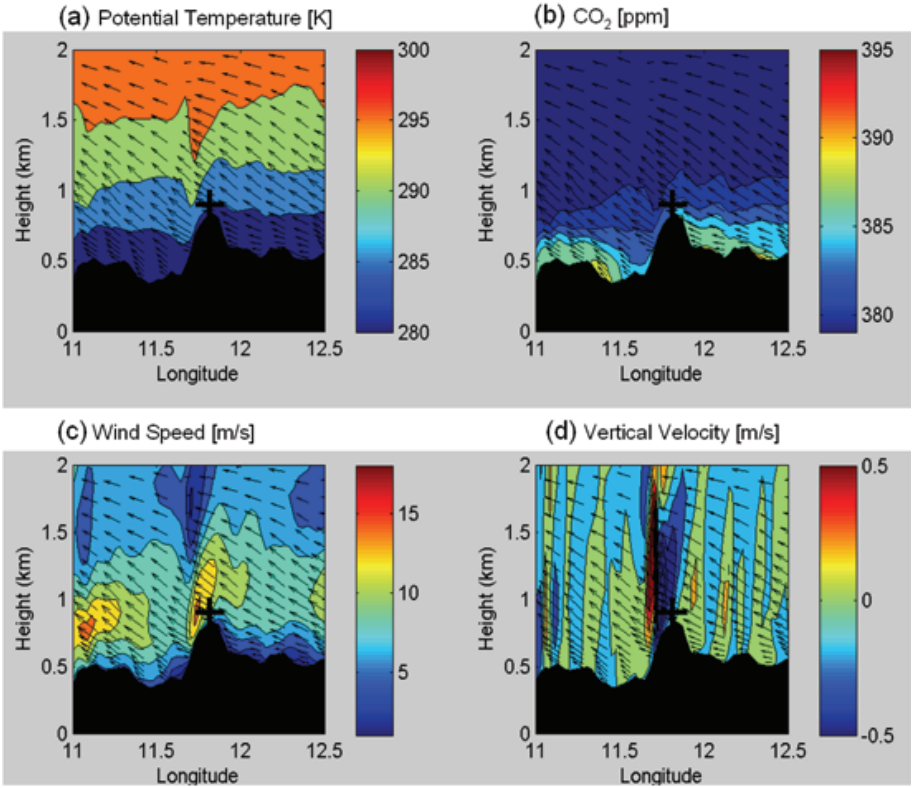

Fig. 12. Vertical cross section along OXK latitude (50°01′ N) on 17 October 2006 at 02:00 UTC, showing WRF-VPRM simulated **(a)** potential temperature in Kelvin, **(b)** CO_2 concentration in ppm, **(c)** wind speed in $m\,s^{-1}$, and **(d)** vertical velocity in $m\,s^{-1}$. The overlaid arrows indicate wind direction.

ACPD
11, 6875–6917, 2011

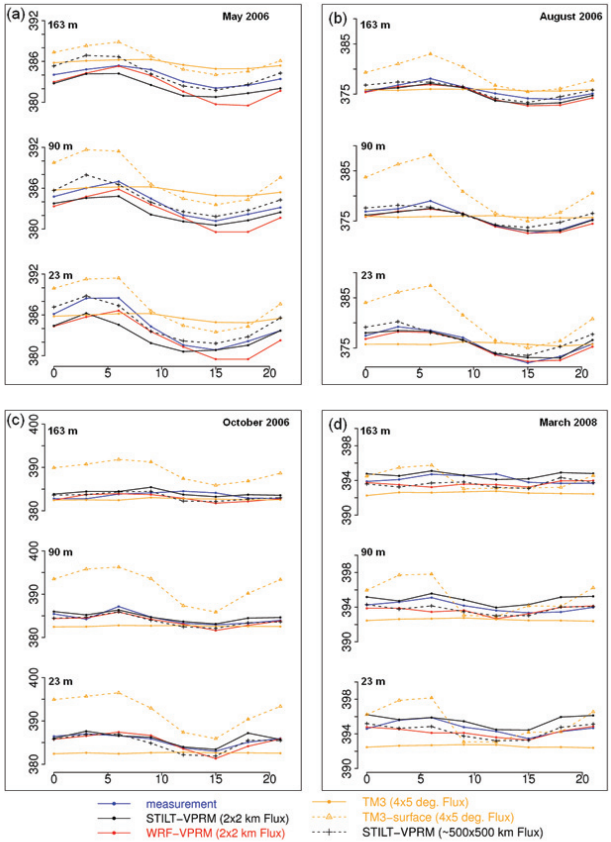

Fig. 13. Averaged diurnal cycle of observed and modeled CO_2 for OXK at different measurement levels and for different seasons: **(a)** May 2006 (spring), **(b)** August 2006 (summer), **(c)** October 2006 (autumn), and **(d)** March 2008 (winter). In each plots, top to bottom panels represents CO_2 at 163 m, 90 m and 23 m, respectively. *X*-axis: hour; *Y*-axis: CO_2 concentration in ppm.

ACPD
11, 6875–6917, 2011